SCIENTIFIC REPORTS

OPEN

SUBJECT AREAS:
NANOSCALE MATERIALS
ELECTROCATALYSIS

Received
13 January 2014

Accepted
30 May 2014

Published
26 June 2014

Correspondence and requests for materials should be addressed to H.P. (huipan@umac.mo)

Metal Dichalcogenides Monolayers: Novel Catalysts for Electrochemical Hydrogen Production

Hui Pan

Institute of Applied Physics and Materials Engineering, Faculty of Science and Technology, University of Macau, Macau SAR, China.

Catalyst-driven electrolysis of water is considered as a "cleanest" way for hydrogen production. Finding cheap and abundant catalysts is critical to the large-scale implementation of the technology. Two-dimensional metal dichalcogenides nanostructures have attracted increasing attention because of their catalytic performances in water electrolysis. In this work, we systematically investigate the hydrogen evolution reduction of metal dichalcogenides monolayers based on density-functional-theory calculations. We find that metal disulfide monolayers show better catalytic performance on hydrogen production than other metal dichalcogenides. We show that their hydrogen evolution reduction strongly depends on the hydrogen coverage and the catalytic performance reduces with the increment of coverage because of hydrogenation-induced lower conductivity. We further show that the catalytic performance of vanadium disulfide monolayer is comparable to that of Pt at lower hydrogen coverage and the performance at higher coverage can be improved by hybridizing with conducting nanomaterials to enhance conductivity. These metal disulfide monolayers with lower overpotentials may apply to water electrolysis for hydrogen production.

Energy has been a key in the development of every sphere of human society. The traditional usable energy sources, including fossil fuels and coal, will fall short of the demand of sustainable development over the long term, and their continued use produces harmful side effects such as pollution that threatens human health and greenhouse gases associated with climate change, which have triggered considerable world-wide effort to explore renewable green energy alternatives[1]. Hydrogen is considered to be one of the most important candidates because of its abundance and clean and renewable nature. As an ideal clean energy carrier for future, hydrogen can be produced from a variety of energy resources, has the highest energy density per unit mass, and produce the least polluting since it can be extracted from natural resource such as water or biomass and its use produces water only. The electrolysis of water is considered as a well-known principle to produce oxygen and hydrogen gas in a sustainable fashion[2–6]. The key component in electrochemical reduction of water is the catalyst for hydrogen evolution reduction (HER). The well-known catalysts in the electrolysis of water are noble metals, such as platinum, due to their superior electrocatalytic properties[7–10]. The application of noble metal catalysts in large-scale production of hydrogen is limited by their high cost and low abundance, although lots of efforts had been done by tuning the composition of the catalyst to modify their electronic structures[11–24]. On the other hands, considerable efforts have been carried out to search alternative catalysts with lower cost and abundance[22–25]. Basically, an advanced catalyst for the enhanced electrochemical hydrogen evolution reaction should reduce the HER reaction overpotential and consequently increase the HER efficiency[3–6,25].

The transition-metal dichalcogenides with the formula of MX_2, where M is a transition metal element from group IV (Ti, Zr, or Hf), group V (for instance V, Nb or Ta) or group VI (Mo or W), and X is a chalcogen (S, Se or Te), have attracted increasing attention for their applications in electrolysis of water[26–43]. These materials have crystal structures consisting of weakly coupled sandwich layers *X*-M-*X*, where one M-atom layer is enclosed within two X layers and the atoms in layers are hexagonally packed[43]. The overall symmetry of transition metal dichalcogenides can be hexagonal or rhombohedral, and the metal atoms have octahedral (1T) or trigonal prismatic (2H) coordination[43]. Experimental and theoretical studies had suggested that the electrocatalytical activity of 2H-MoS_2 in electrolysis of water is contributed to its edges[27–29], which are metallic if they are zigzag[44,45]. Recently, Voiry et al.[37] reported that metallic 1T-WS_2 nanosheets showed better HER performance than semiconducting 2H-WS_2, which can be further improved by strain engineering. As compared with the noble metals, we may be sure that only MX_2 monolayers with high conductivity, and MX_2 nanoribbons/nanoparticles with

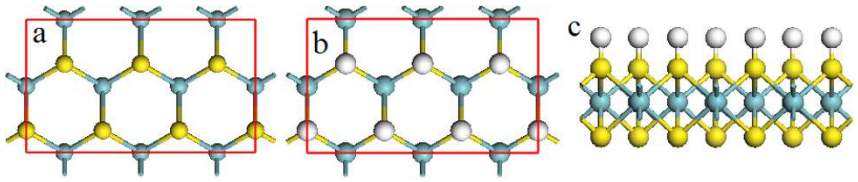

Figure 1 | The representative structures of pristine MX_2 (a) and fully H-covered MX_2 (b) top and (c) side views.

metallic edges can promise the excellent HER activity. To date, a comprehensive study on the HER performances of MX_2 monolayers as well as its origin has not been available. In this work, the applications of MX_2 monolayers in electrolysis of water are systematically investigated based on the calculations of density-functional theory (DFT). We predict that the HER performances of MX_2 monolayers depend on M, X and H-coverage. We show that VS_2 is comparable to Pt for electrolysis of water at lower H-coverage and its catalytic activity can be further enhanced by improving conductivity.

Results and discussion

In our calculations, we focus on metallic/semimetallic 2H transition-metal dichalcogenides, MX_2 (M = Nb, Ta, and V; X = S, Se, and Te) because 2H phase is more stable and high conductivity is essential to the electrolysis of water. The MX_2 unit cells with trigonal prismatic (2H) coordination are first optimized to obtain the lattice parameters. The optimized structures of MX_2 (M = Nb, and Ta; X = S, Se, and Te) (see Supporting Data, Table I) from our calculations are consistent with the reported experimental and theoretical data[46]. We see that the lattice parameters of NbX_2 are almost equivalent to those of TaX_2, while are larger than those of VX_2 (Supporting Data, Table I). To investigate the HER performances of MX_2 monolayers at various hydrogen coverage on their surfaces, the geometries of MX_2 monolayers with one surface fully covered by hydrogen atoms (MX_2-H) are relaxed to find out the effects of hydrogen coverage on their lattice parameters. The hydrogen atoms are adsorbed on the top of X atoms (Figure 1), where is the most stable position[37,47,48]. The optimized structures of MX_2-H (Table II in Supporting Data & Figure 2) show that the lattice constants (a) are extended by 2.0 to 3.8%, 1.7 to 3.3%, and 3.4 to 4.5% for NbX_2, TaX_2, and VX_2, respectively, where the extension increases as X changes for S to Se, further to Te (Figure 2). The thicknesses (c) and the X-M bonds of the monolayers are reduced by the H-coverage on their surfaces (Figure 2). The calculated bond lengths are about 1.4, 1.5 and 1.7 Å for S-H, Se-H, and Te-H bonding, respectively (Supporting Data, Table II).

According to the Sabatier principle, the optimal catalytic activity of material for HER can be achieved on a catalytic surface with intermediate binding energies (or free energies of adsorption) for reactive intermediates[15], which can be quantified by analyzing the reaction free energy of hydrogen adsorption (ΔG_H)[13,15,37,49]. The optimum value is around $\Delta G_H = 0$. To obtain the reaction free energy, we calculate ΔG_H for various H coverage on MX_2 monolayers as following:

$$\Delta G_H = \Delta E_H + \Delta E_{ZPE} - T\Delta S_H \quad (1)$$

where ΔE_H is the hydrogen chemisorption energy defined as:

$$\Delta E_H = E(MX_2 + nH) - E(MX_2 + (n-1)H) - \frac{1}{2}E(H_2) \quad (2)$$

where n is the number of H atoms adsorbed on a MX_2 monolayer. Full coverage refers to one hydrogen atom per X atom adsorbed on one side of the MX_2 monolayer. The ΔG_H as a function of the hydrogen coverage can be obtained by changing n. $E(MX_2 + nH)$, $E(MX_2)$ and $E(H_2)$ in Eq. (2) are the energies of monolayer with hydrogen atoms (n), pure MX_2 monolayer (n = 1), and hydrogen molecule, respectively. ΔS_H is the difference in entropy. The entropy of adsorption of 1/2 H_2 is $\Delta S_H \cong -1/2S^0_{H_2}$, where $S^0_{H_2}$ is the entropy of H_2 in the gas phase at standard conditions. ΔE_{ZPE} is the difference in zero point energy between the adsorbed and the gas phase, related to the reaction: $1/2H_2(g) \rightarrow H^*$, where H^* denotes a hydrogen atom adsorbed on the surface. $\Delta E_{ZPE} - T\Delta S_H$ is about 0.24 eV[13,37,49], simplifying Eq. (1) to $\Delta G_H = \Delta E_H + 0.24$.

Rectangle supercell (Figure 1) is employed to study the different hydrogen coverage on MX_2 monolayer, $\frac{i}{6}(i = 1 \sim 6)$. The full coverage ($\frac{6}{6}$ *or* 1) is that all of X atoms on one side of the monolayer adsorb hydrogen atoms (Figures 1b&1c). A supercell with double size in y direction of Figure 1 is used for $\frac{1}{12}$ coverage, that is, one H atom is attached to one of the 12 X atoms. $\frac{1}{6}$ coverage is that one H atom is attached to one of the 6 X atoms (Figure 1). For other coverage ($\frac{i}{6}(i = 2 \sim 5)$), all of the possible H-adsorption configurations on the six X atoms are considered, where the adsorption energy is calculated by two methods – "average" of all configurations and "most stable" configuration. We first consider the supercell (p-supercell) based on monolayer pristine lattice parameters (from Table I in Supporting Data). The calculated adsorption energies show that the overpotentials are positive, and ΔG_H increases with the increase of H coverage on the MX_2 monolayer (Figure 3), which is in contrast with that of Pt (ΔG_H trends on zero with the increase of H coverage)[13,15,49]. We see that the calculated ΔG_H follows the same trend regardless of the calculation methods (Figures 3a, 3c, and 3e for "average" method, and Figures 3b, 3d, and 3f for "most stable" method) and the difference on values induced by the method is minor. Importantly, the ΔG_H of MS_2 is lower than those of MSe_2 and MTe_2 by 40% at the same H coverage (Figure 3), indicating that the HER performances of MS_2 monolayers are better than those of MSe_2 and MTe_2 monolayers. The overpotentials at $\frac{1}{12}$ coverage from "average" method (Figures 3a, 3c, & 3e) are 0.061, 0.192, and 0.007 eV for NbS_2, TaS_2, and VS_2, respectively. At $\frac{1}{6}$ coverage, the ΔG_H for NbS_2, TaS_2, and VS_2 are 0.112, 0.266, and 0.051 eV, respect-

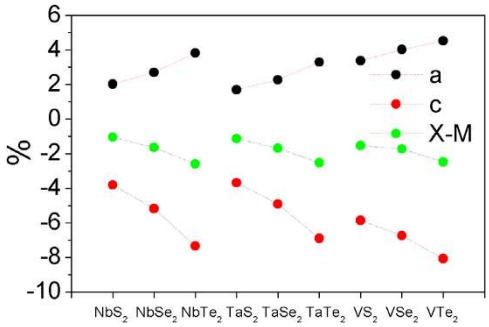

Figure 2 | The difference of lattice parameters, including lattice constant (a), monolayer's thickness (c), and X-M bond length (X-M), between pristine and H-covered MX_2 monolayers.

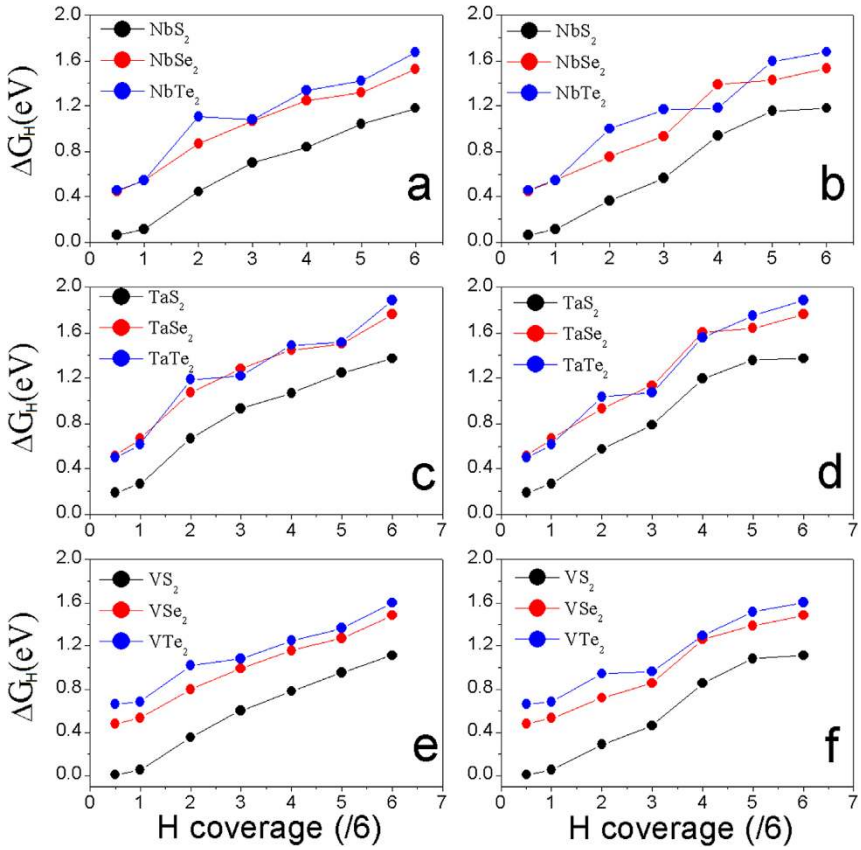

Figure 3 | The calculated overpotentials as a function of H-coverage of MX_2 monolayers in p-supercell by "average" method: (a), (c), and (e); and by "most stable" method: (b), (d) and (f).

ively. We see that the HER performances of NbS_2, TaS_2, and VS_2 monolayers are better than that of 1T-WS_2 monolayer because their ΔG_H at relatively high H-coverage is lower than that of 1T-WS_2 at lower H-coverage (ΔG_H = 0.28 eV at $\frac{1}{16}$ coverage and ΔG_H = 0.36 eV at $\frac{2}{16}$ coverage)[37]. The HER performance of VS_2 at a coverage up to $\frac{1}{6}$ is also better than that of MoS_2 edges (ΔG_H = 0.08 eV)[28]. For comparison, we compose the curves of ΔG_H of MS_2 (M = Nb, Ta, and V) monolayers as a function of H-coverage into Figure 4a. We see that the HER performances of MS_2 monolayers increase as M changes from Ta to Nb, further to V. The overpotential of VS_2 at $\frac{1}{12}$ coverage is 10 and 30 times lower than those of NbS_2 and TaS_2. The VS_2-based catalyst for electrolysis of water may be comparable to that of Pt at lower H-coverage (up to $\frac{1}{12}$ coverage) because of its near-zero overpotential (0.007 eV). The difference at HER performance, however, decreases with the increase of H-coverage on the monolayer. At full coverage ($\frac{6}{6}$ *or* 1), VS_2 only take advantage of NbS_2 and TaS_2 by 6 and 20%, respectively.

We also calculate the hydrogen adsorption energy in the supercell (h-supercell) constructed on the lattice parameters of fully H-covered monolayer (from Table II in Supporting Data). We see that the HER trend as a function of H-coverage (Figure 5) is the same as that in p-supercell. The MS_2 monolayers still show the best HER performance at same H-coverage because their overpotentials are smaller than those of MSe_2 and MTe_2 monolayers (Figure 5). For all of MX_2 monolayers, ΔG_H in h-supercell is reduced because of the extended lattice constants (that is equivalent to the effect of strain in Ref. 37). The difference of ΔG_H between p-supercell and h-supercell, however, becomes smaller as the H-coverage increases, indicating that the strain shows less effect on HER of the monolayer if the H-coverage is high. At $\frac{1}{12}$ coverage, the overpotentials from "average" method (Figures 5a, 5c, & 5e) are −0.07, 0.098, and −0.159 eV for NbS_2, TaS_2, and VS_2, respectively, and at $\frac{1}{6}$ coverage, the corresponding ΔG_H are 0.004, 0.174, and −0.138 eV, respectively, which should imply that NbS_2 shows the best HER performance at lover H-coverage in h-supercell. With the increase of H-coverage on the MS_2 monolayers' surfaces, ΔG_H increases (Figure 4b). After 25% H-coverage, VS_2 gives out the best HER performance because its overpotential is positive and lower than those of NbS_2 and TaS_2 (Figure 4b). By carefully comparing the energies of systems calculated from p-supercell and h-supercell, we find that the effect of H-coverage on lattice parameters is negligible when it is less than the 33% ($\frac{2}{6}$coverage). Therefore, we combine the calculated ΔG_H of MS_2 from p-supercell for H-coverage up to $\frac{1}{6}$ and h-supercell for H-coverage from $\frac{2}{6}$ to $\frac{6}{6}$ into Figure 6. Clearly, we see that VS_2 monolayer shows the best HER performance in all of considered systems.

To investigate the possible origin of HER performance and the effects of H-coverage, the partial densities of states (PDOSs) of M, X, and H are calculated. The calculated PDOSs clearly show the change of conductivities of MS_2 monolayers with the H-coverage (Figure 7 and supporting data S1 ~ S5). We see that the pristine VS_2 monolayer is metallic, where the Fermi level is within the middle energy band and near to its bottom (Figure 7a). The middle energy states are dominated by V *d* electrons. With introducing H atoms to the monolayer's surface, the energy sates shift down to lower energy region, or

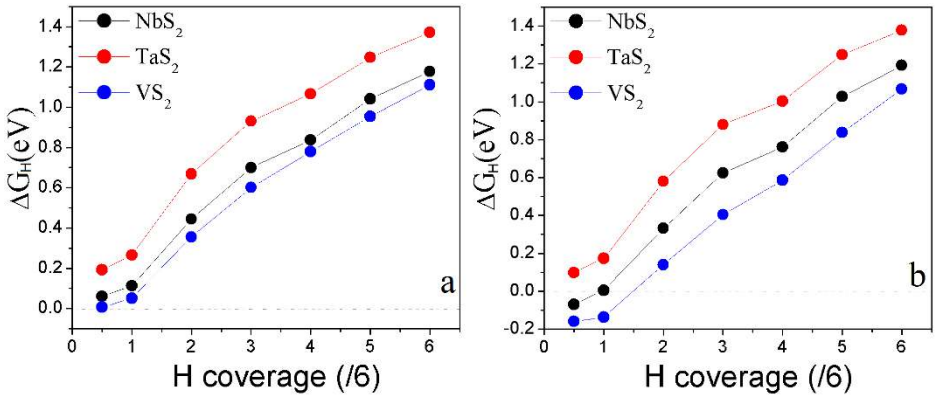

Figure 4 | The calculated overpotentials as a function of H-coverage of MS_2 monolayers by "average" method in p-supercell (a) and in h-supercell (b).

the Fermi level shifts up to high energy region within the middle band (Figure 7b). The Fermi level further shifts up with increasing H-coverage (Figure 7c ~ h). At $\frac{3}{6}$ coverage, the Fermi level of the system is close to the middle energy band top. Corresponding to semiconductor's band structure, we may state the middle band as valence band and the band above as conduction band. The up-shift of Fermi level to the middle band (valence band) top leads to the reduction of conductivity. This is further illustrated on VS_2 monolayer with full H-coverage, where the system is an intrinsic semiconductor or insulator because its Fermi level is within the band gap (Figure 7h). The PDOSs of NbS_2 and TaS_2 in p-supercell and h-supercell, and VS_2 in h-supercell reveal the same origin of the reduction of performance under high H-coverage (Supporting data, S1 ~ S5). The analysis of PDOSs shows that the conductivities of the MX_2 monolayers are reduced by the H-coverage, especially after half H-coverage on the surfaces, leading to the decreases of their HER performances (Figures 3 ~ 6). This finding may also apply to the MX_2 nanostructures with metallic edges because their conductivities should be reduced when edges are fully saturated by hydrogen atoms[44]. This is different from Pt-related catalysts, whose conductivities have not been affected by the H-coverage on their surfaces[13,15,49]. How to improve the conductivities of MS_2-based catalysts under high H-coverage should be a challenge for their application in electrolysis of water. One of ways is to mix these MS_2 monolayers with high conducting nanostructures, such as graphene[33,50].

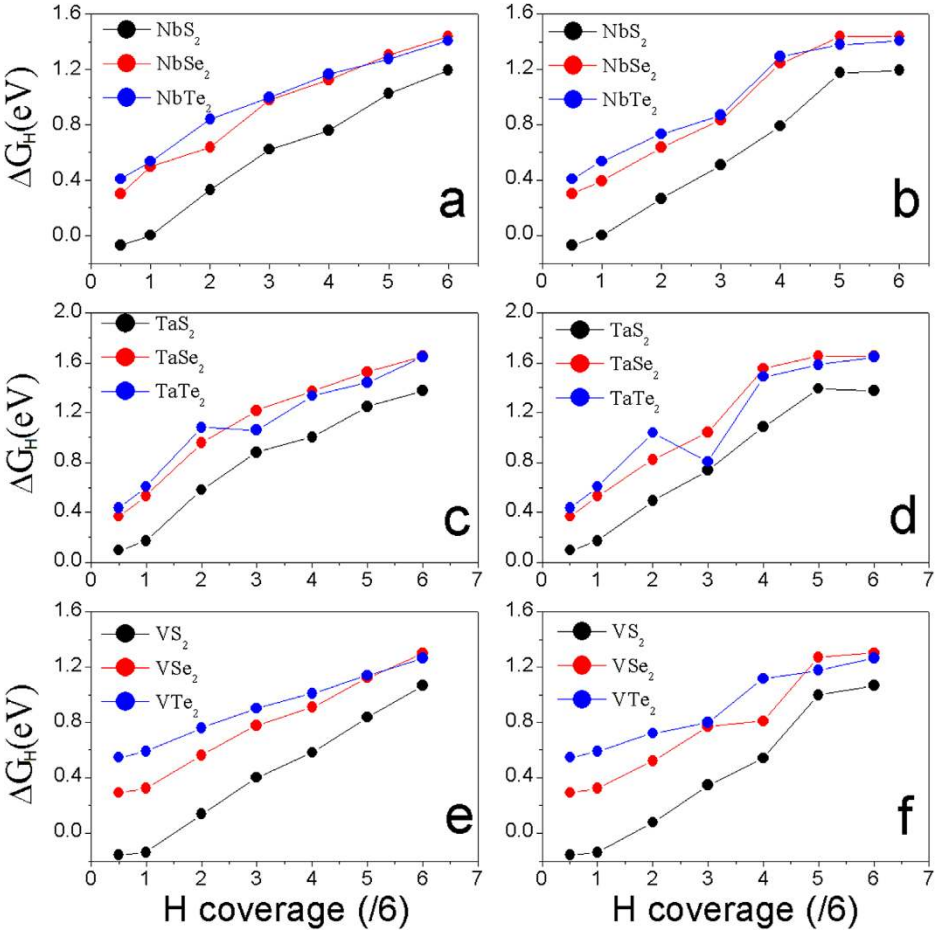

Figure 5 | The calculated overpotentials as a function of H-coverage of MX_2 monolayers in h-supercell by "average" method: (a), (c), and (e); and by "most stable" method: (b), (d) and (f).

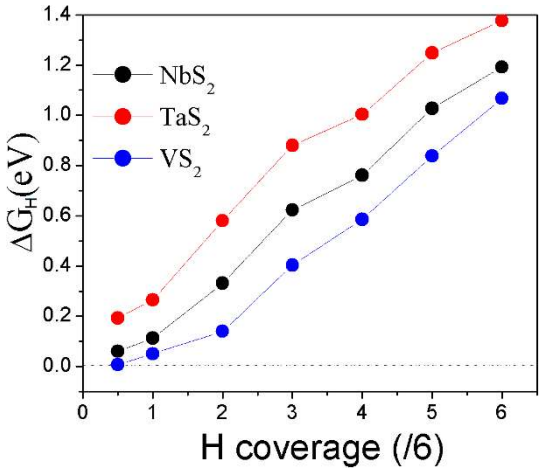

Figure 6 | The combined overpotentials as a function of H-coverage of MS_2 monolayers by "average" method in p-supercell (H-coverage $< \frac{2}{6}$) and in h-supercell (H-coverage $\geq \frac{2}{6}$).

For comparison, the HER performance of MoS_2 monolayer is calculated. We see that its overpotential (ΔG_H) (Supporting data, S6) is larger than those of MX_2 (M = Nb, Ta, and V; X = S, Se, and Te) monolayers considered in this work (Figure 6). At lower and full H-coverage ($\frac{1}{12}$, $\frac{1}{6}$, and 1), its overpotential is about 2.0 ~ 2.1 eV. At moderate H-coverage, its overpotential is larger than 1.1 eV. The calculated densities of states show that pure and H-covered MoS_2 monolayers are intrinsic or n-type semiconductors (Supporting data, S7). These results confirm that the surface of MoS_2 monolayer is inert to electrolysis of water, and the most active sites are at the edges or defects of MoS_2 nanostructures[27–29]. However, our study show that the surfaces of MX_2 (M = Nb, Ta, and V; X = S, Se, and Te) monolayers, especially VS_2, are very active, which further enhance their ability for electrolysis of water due to higher contacting area with water.

Conclusions

The DFT-based first-principles calculations are carried out to investigate the hydrogen evolution reduction of MX_2 monolayers. We find that MS_2 monolayers are better than MSe_2 and MTe_2 monolayers in electrolysis of water, especially VS_2, which shows the best HER performance because of its lower overpotential. We show that the HER performances of MX_2 monolayers strongly depend on the H-coverage on their surfaces. With increasing H-coverage, the performance is reduced because of the reduction of conductivity. We also show that the strain may improve the HER performance at relatively low H-coverage. We further predict that their HER applications at high H-coverage can also be achieved by improving their conductivities, such as hybridization with metallic nanostructures. It is expected that the MS_2 monolayers, especially VS_2, may find applications to electrolysis of water for hydrogen production.

Methods

The first-principles calculations are carried out to investigate the hydrogen evolution reduction of transition-metal dichalcogenide monolayers. Our calculations are based on the density functional theory (DFT)[51] and the Perdew-Burke-Ernerhof generalized gradient approximation (PBE-GGA)[52]. The projector augmented wave (PAW) scheme[53,54] as incorporated in the Vienna ab initio simulation package (VASP)[55] is used in the study. The Monkhorst and Pack scheme of k point sampling is used for integration over the first Brillouin zone[56]. A $15 \times 15 \times 1$ grid for k-point sampling for geometry optimization of unit cells, and an energy cut-off of 450 eV are consistently used in our calculations. A sufficiently large supercell is used so that the monolayers in neighbouring cells in the vertical direction are separated by a vacuum region of at least 20 Å. Good convergence is obtained with these parameters and the total energy was converged to 2.0×10^{-5} eV/atom. The error bar (or uncertainty) of the DFT calculation is less than 5 meV. The thermodynamic processes via Tafel pathway are calculated[17]. The effect of solvent on the HER performance of VS_2 monolayer is investigated by including H_2O molecules in the systems with various H-coverage[18,21].

The calculated thermodynamc processes of HER on VS_2 monolayer via Tafel channels and the effect of solvent on overpotentials are included in Supporting Data.

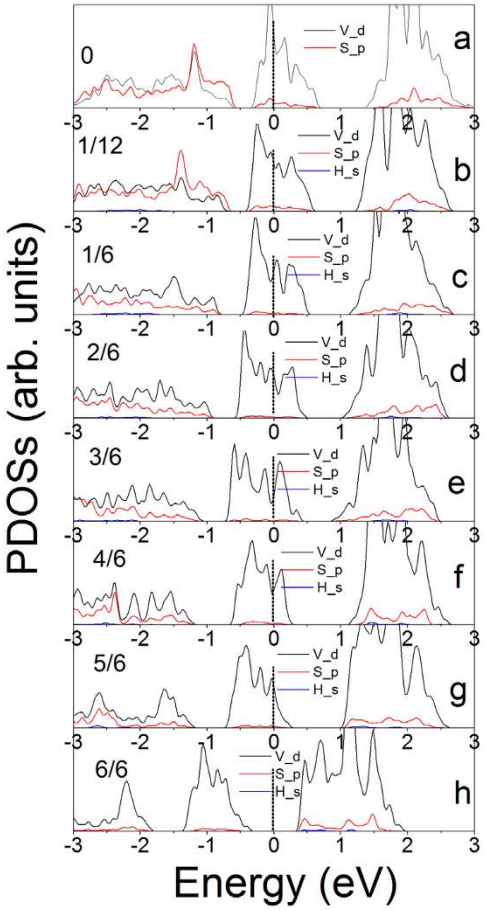

Figure 7 | The calculated partial densities of states of pristine (a) and various H-covered (b ~ h) VS_2 monolayers in p-supercell.

1. Lewis, N. S., Crabtree, G., Nozik, A. J., Wasielewski, M. R. & Alivisatos, P. Basic Research Needs for Solar Energy Utilization, Report of Department of Energy, USA (2005), Date of access: 01/12/2013. http://science.energy.gov/bes/news-and-resources/reports/abstracts/#SEU.
2. Kreuter, W. & Hofmann, H. Electrolysis: the important energy transformer in a world of sustainable energy. *Int. J. Hydrogen Energy* **23**, 661–666 (1998).
3. Suffredini, H. B., Cerne, J. L., Crnkovic, F. C., Machado, S. A. S. & Avaca, L. A. Recent developments in electrode materials for water electrolysis. *Int. J. Hydrogen Energy* **25**, 415–423 (2000).
4. Christopher, K. & Dimitrios, R. A review on exergy comparison of hydrogen production methods from renewable energy sources. *Energy Environ. Sci.* **5**, 6640–6651 (2012).
5. Holladay, J. D., Hu, J., King, D. L. & Wang, Y. An overview of hydrogen production technologies. *Catal. Today* **139**, 244–260 (2009).
6. Carmo, M., Fritz, D. L., Merge, J. & Stolten, D. A comprehensive review on PEM water electrolysis. *Int. J. Hydrogen Energy* **38**, 4901–4934 (2013).
7. Sheng, W., Gasteiger, H. A. & Shao-Horn, Y. Hydrogen oxidation and evolution reaction kinetics on platinum: acid vs alkaline electrolytes. *J. Electrochem. Soc.* **157**, B1529–B1536 (2010).
8. Fang, Y. H. & Liu, Z. P. Surface phase diagram and oxygen coupling kinetics on flat and stepped Pt surfaces under electrochemical potentials. *J. Phys. Chem. C* **113**, 9765–9772 (2009).
9. Kwon, G. *et al.* Size-dependent subnanometer Pd cluster (Pd-4, Pd-6, and Pd-17) water oxidation electrocatalysis. *ACS Nano* **7**, 5808–5817 (2013).
10. Jiang, L., Myer, B., Tellefsen, K. & Pau, S. A planar microfabricated electrolyzer for hydrogen and oxygen generation. *J. Power Sources* **188**, 256–260 (2009).
11. Stamenkovic, V. R. *et al.* Improved Oxygen Reduction Activity on $Pt_3Ni(111)$ via Increased Surface Site Availability. *Science* **315**, 493–497 (2007).
12. Zhang, J., Sasaki, K., Sutter, E. & Adzic, R. R. Stabilization of Platinum Oxygen-Reduction Electrocatalysts Using Gold Clusters. *Science* **315**, 220–222 (2007).

13. Pan, H., Feng, Y. P. & Lin, J. Y. Enhancement of hydrogen evolution on tungsten doped platinum. *J. Comput. Theor. Nanosci.* **7**, 547–551 (2010).
14. Koh, S. & Strasser, P. Electrocatalysis on bimetallic surfaces: modifying catalytic reactivity for oxygen reduction by voltammetric surface dealloying. *J. Am. Chem. Soc.* **129**, 12624–12625 (2007).
15. Gressley, J., Jarmaillo, T. F., Bonde, J., Chorkendorff, I. & Nørskov, J. K. Computational high-throughput screening of electrocatalytic materials for hydrogen evolution. *Nature Mater.* **5**, 909–913 (2006).
16. Hu, W. K. & Lee, J. Y. Electrocatalytic properties of Ti_2Ni/Ni-Mo composite electrodes for hydrogen evolution reaction. *Int. J. Hydro. Energy* **23**, 253–257 (1998).
17. Fang, Y. H., Wei, G. F. & Liu, Z. P. Catalytic role of minority species and minority sites for electrochemical hydrogen evolution on metals: surface charging, coverage, and Tafel kinetics. *J. Phys. Chem. C* **117**, 7669–7680 (2013).
18. Rossmeisl, J., Logadottir, A. & Nørskov, J. K. Electrolysis of water on (oxidized) metal surfaces. *Chem. Phys.* **319**, 178–184 (2005).
19. Fang, Y. H. & Liu, Z. P. Toward anticorrosion electrodes: site-selectivity and self-acceleration in the electrochemical corrosion of Platinum. *J. Phys. Chem. C* **114**, 4057–4062 (2010).
20. Wei, G. F. & Liu, Z. P. Towards active and stable oxygen reduction cathodes: a density functional theory survey on Pt_2M skin alloys. *Energy Environ. Sci.* **4**, 1268–1272 (2011).
21. Fang, Y. H., Wei, G. F. & Liu, Z. P. Theoretical modeling of electrode/electrolyte interface from first-principles periodic continuum solvation method. *Catal. Today* **202**, 98–104 (2013).
22. Wu, M., Shen, P. K., Wei, Z. D., Song, S. Q., & Nie, M. High activity PtPd-WC/C electrocatalyst for hydrogen evolution reaction. *J. Power Sources* **166**, 310–316 (2007).
23. Esposito, D. V., Hunt, S. T., Kimmel, Y. C. & Chen, J. G. G. A new class of electrocatalysts for hydrogen production from water electrolysis: metal monolayers supported on low-Cost transition metal carbides. *J. Am. Chem. Soc.* **134**, 3025–3033 (2012).
24. Zheng, Z. *et al.* Electrochemical synthesis of Ni-S/CeO_2 composite electrodes for hydrogen evolution reaction. *J. Power Sources* **230**, 10–14 (2013).
25. Chen, W. F., Muckerman, J. T. & Fujita, E. Recent developments in transition metal carbides and nitrides as hydrogen evolution electrocatalysts. *Chem. Commun.* **49**, 8896–8909 (2013).
26. Laursen, L. B., Kegnæs, S., Dahla, S. & Chorkendorff, I. Molybdenum sulphides efficient and viable materials for electro- and photoelectrocatalytic hydrogen evolution. *Energy Environ. Sci.* **5**, 5577–5591 (2012).
27. Hinnemann, B. *et al.* Biomimetic hydrogen evolution: MoS_2 nanoparticles as catalyst for hydrogen evolution. *J. Am. Chem. Soc.* **127**, 5308–5309 (2005).
28. Jaramillo, T. F. *et al.* Identification of active edge sites for electrochemical H_2 evolution from MoS_2 nanocatalysts. *Science* **317**, 100–102 (2007).
29. Karunadasa, H. I. *et al.* Molecular MoS_2 edge site mimic for catalytic hydrogen generation. *Science* **335**, 698–702 (2012).
30. Merki, D., Fierro, S., Vrubel, H. & Hu, X. Amorphous molybdenum sulphide films as catalysts for electrochemical hydrogen production in water. *Chem. Sci.* **2**, 1262–1267 (2011).
31. Vrubel, H., Merki, D. & Hu, X. Hydrogen evolution catalyzed by MoS_3 and MoS_2 particles. *Energy Environ. Sci.* **5**, 6136–6144 (2012).
32. Kibsgaard, J., Chen, Z., Reinecke, B. N. & Jaramillo, T. F. Engineering the surface structure of MoS2 to preferentially expose active edge sites for electrocatalysis. *Nature Mater.* **11**, 963–969 (2012).
33. Li, Y. *et al.* MoS_2 nanoparticles grown on graphene: An advanced catalyst for the hydrogen evolution reaction. *J. Am. Chem. Soc.* **133**, 7296–7299 (2011).
34. Lukowski, M. A. *et al.* Enhanced hydrogen evolution catalysis from chemically exfoliated metallic MoS_2 nanosheets. *J. Am. Chem. Soc.* **135**, 10274–10277 (2013).
35. Kong, D. *et al.* Synthesis of MoS_2 and $MoSe_2$ films with vertically aligned layers. *Nano Lett.* **13**, 1341–1347 (2013).
36. Wang, H. *et al.* $MoSe_2$ and WSe_2 nanofilms with vertically aligned molecular layers on curved and rough surfaces. *Nano Lett.* **13**, 3426–3433 (2013).
37. Voiry, D. *et al.* Enhanced catalytic activity in strained chemically exfoliated WS_2 nanosheets for hydrogen evolution. *Nature Mater.* **13**, 850–855 (2013).
38. Kong, D. S., Cha, J. J., Wang, H. T., Lee, H. R. & Cui, Y. First-row transition metal dichalcogenide catalysts for hydrogen evolution reaction. *Energy Environ. Sci.* **6**, 3553–3558 (2013).
39. Wang, D. Z. *et al.* Distorted MoS_2 nanostructures: An efficient catalyst for the electrochemical hydrogen evolution reaction. *Electrochem. Commun.* **34**, 219–222 (2013).
40. Wang, T. Y. *et al.* Enhanced electrocatalytic activity for hydrogen evolution reaction from self-assembled monodispersed molybdenum sulfide nanoparticles on an Au electrode. *Energy Environ. Sci.* **6**, 625–633 (2013).
41. Wu, Z. Z. *et al.* MoS_2 nanosheets: a designed structure with high active site density for the hydrogen evolution reaction. *ACS Catal.* **3**, 2101–2107 (2013).
42. Chen, T. Y. *et al.* Comparative study on MoS_2 and WS_2 for electrocatalytic water splitting. *Int. J. Hydro. Energy* **38**, 12302–12309 (2013).
43. Chhowall, M. *et al.* The chemistry of two-dimensional layered transition metal dichalcogenide nanosheets. *Nature Chem.* **5**, 263–275 (2013).
44. Pan, H. & Zhang, Y. W. Edge-dependent structural, electronic and magnetic properties of MoS_2 nanoribbons. *J. Mater. Chem.* **22**, 7280–7290 (2012).
45. Li, Y. F., Zhou, Z., Zhang, S. B. & Chen, Z. F. MoS_2 Nanoribbons: High Stability and Unusual Electronic and Magnetic Properties. *J. Am. Chem. Soc.* **130**, 16739–16744 (2008).
46. Ding, Y. *et al.* First principles study of structural, vibrational and electronic properties of graphene-like MX_2 (M = Mo, Nb, W, Ta; X = S, Se, Te) monolayers. *Physica B* **406**, 2254–2260 (2011).
47. Koh, E. W. K., Chiu, C. H., Lim, Y. K., Zhang, Y. W. & Pan, H. Hydrogen adsorption on and diffusion through MoS_2 monolayer: First-principles study. *Int. J. Hydro. Energy* **37**, 14323–14328 (2012).
48. Shi, H., Pan, H., Zhang, Y. W. & Yakobson, B. I. Strong ferromagnetism in hydrogenated monolayer MoS_2 tuned by strain. *Phys. Rev. B* **88**, 205305 (2013).
49. Nørskov, J. K. *et al.* Trends in the exchange current for hydrogen evolution. *J. Electrochem. Soc.* **152**, J23–J26 (2005).
50. Min, S. X. & Lu, G. X. Sites for high efficient photocatalytic hydrogen evolution on a limited-layered MoS_2 cocatalyst confined on graphene dheets-The role of graphene. *J. Phys. Chem. C* **116**, 25415–25424 (2012).
51. Hohenberg, P. & Kohn, W. Inhomogeneous electron gas. *Phys. Rev.* **136**, B864–B871 (1964).
52. Blöchl, P. E. Projector augmented-wave method. *Phys. Rev. B* **50**, 17953–17979 (1994).
53. Perdew, J. P., Burke, K. & Ernzerhof, M. Generalized gradient approximation made simple. *Phys. Rev. Lett.* **77**, 3865–3868 (1996).
54. Kresse, G. & Joubert, D. From ultrasoft pseudopotentials to the projector augmented-wave method. *Phys. Rev. B* **59**, 1758–1775 (1999).
55. Kresse, G. & Furthmuller, J. Efficient iterative schemes for ab initio total-energy calculations using a plane-wave basis set. *Phys. Rev. B* **54**, 11169–11186 (1996).
56. Monkhorst, H. J. & Pack, J. Special points for brillouin-zone integrations. *Phys. Rev. B* **13**, 5188–5192 (1976).

Acknowledgments

Hui Pan thanks the support of the Science and Technology Development Fund from Macau SAR (FDCT-076/2013/A), and Multi-Year Research Grant (MYRG2014-00159-FST) and Start-up Research Grant (SRG-2013-00033-FST) from Research & Development Office at University of Macau. The DFT calculations were performed at High Performance Computing Cluster (HPCC) of Information and Communication Technology Office (ICTO) at University of Macau.

Author contributions

H.P. conceived the idea, performed the calculations, and wrote the paper.

Additional information

Supplementary information accompanies this paper at http://www.nature.com/scientificreports

Competing financial interests: The authors declare no competing financial interests.

How to cite this article: Pan, H. Metal Dichalcogenides Monolayers: Novel Catalysts for Electrochemical Hydrogen Production. *Sci. Rep.* **4**, 5348; DOI:10.1038/srep05348 (2014).